Generalized second-order slip boundary condition for nonequilibrium gas flows

Zhaoli Guo,[1,2,*] Jishun Qin,[3] and Chuguang Zheng[1]

[1]*State Key Laboratory of Coal Combustion, Huazhong University of Science and Technology, Wuhan 430074, China*
[2]*Beijing Computational Science Research Center, Beijing 100084, China*
[3]*State Key Laboratory of Enhanced Oil Recovery, Research Institute of Petroleum Exploration and Development, Beijing 100083, P. R. China*

It is a challenging task to model nonequilibrium gas flows within a continuum-fluid framework. Recently some extended hydrodynamic models in the Navier-Stokes formulation have been developed for such flows. A key problem in the application of such models is that suitable boundary conditions must be specified. In the present work, a generalized second-order slip boundary condition is developed in which an effective mean-free path considering the wall effect is used. By combining this slip scheme with certain extended Navier-Stokes constitutive relation models, we obtained a method for nonequilibrium gas flows with solid boundaries. The method is applied to several rarefied gas flows involving planar or curved walls, including the Kramers' problem, the planar Poiseuille flow, the cylindrical Couette flow, and the low speed flow over a sphere. The results show that the proposed method is able to give satisfied predictions, indicating the good potential of the method for nonequilibrium flows.

　　　　　　PACS number(s): 47.61.−k, 47.45.Gx, 47.11.−j

I. INTRODUCTION

As a gas flows over a solid surface, a kinetic boundary layer, also known as Knudsen layer (KL), will be formed near the surface with a thickness of the order of the mean-free path (λ) of the gas. Outside the KL, the gas flow can be well described by the Navier-Stokes equations; within the KL, however, the gas is very rarefied, and consequently the continuum assumption and the quasithermodynamic-equilibrium assumption, upon which the Navier-Stokes constitution is based, will break down inevitably in this region. Furthermore, within the KL the collisions among gas molecules are relatively rare in comparison with that in the bulk region, and collisions between gas molecules and solid wall are significant. Generally the average gas velocity at the wall is different from that of the surface due to the interactions between the gas and wall molecules, which means a velocity slip occurs. Actually there is ample theoretical, experimental, and numerical evidence that discontinuity or slippage does appear at the surface in rarefied gas systems.

In many real world fluid systems, the domain size L is usually much larger than the mean-free path λ, i.e., Kn $= \lambda/L \ll 1$ (say, Kn $\leqslant 10^{-3}$), where Kn is the Knudsen number. Under such circumstances, the fluid can be treated as a continuum over the whole domain, and the KL takes only a negligible portion of the flow domain, and its effect on the bulk flow outside the KL can be neglected. Therefore, the flow can be well modeled by the Navier-Stokes equations with the no-slip boundary condition. However, if the Knudsen number is relatively large (Kn $> 10^{-3}$), such as low-pressure gas flows at high altitude or flows over microdevices, the effect of the KL on the bulk flow cannot be neglected anymore. Usually, if the gas is not so rarefied ($10^{-3} \leqslant$ Kn < 0.1), the KL effect can be modeled with certain slip boundary conditions, and the classical Navier-Stokes equations can still be used to describe the bulk flow. Regarding the surface slippage, it

should be noted first that two slip velocities can be identified, as shown in Fig. 1. The first one is the microscopic slip velocity, u_s, which is defined as the average velocity of the gas molecules at the surface that can be obtained from kinetic theory [1]. Another slip velocity, u_s^{ns}, is the "apparent" or macroscopic slip velocity, which is defined as the extrapolated value from the velocity of the Navier-Stokes equations in the bulk region. A famous slip boundary condition for flows in slip regime ($10^{-3} <$ Kn < 0.1) is attributed to Maxwell [2], who derived the expression of the slip velocity based on gas kinetic theory:

$$u_s^{ns} = u_g^{ns} - u_w = \frac{2-\sigma}{\sigma}\lambda\frac{\partial u^{ns}}{\partial \boldsymbol{n}}, \tag{1}$$

where $\boldsymbol{n}$ is the unit vector normal to the surface, σ is the tangential momentum accommodation coefficient of the wall, u_g^{ns} is the tangential gas velocity at the surface predicted by the Navier-Stokes equations, and u_w is the tangential wall velocity. A more general formulation of the Maxwell slip boundary condition is to rewrite the normal velocity gradient in terms of the tangential shear stress [3]. The Maxwell's first-order slip boundary condition has been shown to be able to capture accurately bulk flow behaviors if the gas is only slightly rarefied [4–6], but the applications to flows with relatively larger Knudsen numbers are unsatisfied (see Ref. [6] and references therein). Therefore, some second-order slip boundary conditions have been developed to extend the application range of the Navier-Stokes equations [7–11].

For rarefied gas flows far from equilibrium, the KL takes a large portion of the whole domain and dominates the overall flow. The Navier-Stokes equations with slip boundary conditions would not work anymore. Instead, one should resort to either the kinetic model (Boltzmann equation) together with certain kinetic boundary conditions [12–19] or alternative hydrodynamic models beyond the Navier-Stokes equations, such as the Burnett or super-Burnett equations, the Grad 13 moments equations, and the regularized Grad moment equations [20–26]. However, the solving of the Boltzmann equation, either by the deterministic discrete-velocity model
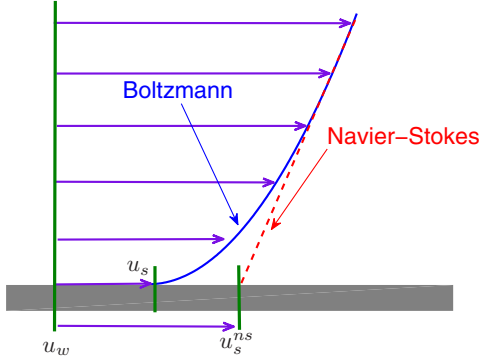
*zlguo@mail.hust.edu.cn

FIG. 1. (Color online) Sketch of the velocity profile in the Knudsen layer.

or by the stochastic direct simulation Monte Carlo (DSMC) method, is rather nontrivial, while the hydrodynamic models beyond Navier-Stokes also have their own difficulties such as the lack of well-posed boundary conditions and the inherent instability. These difficulties have motivated some recent interest in developing extended hydrodynamic models in the Navier-Stokes framework [extended Navier-Stokes (ENS)] for rarefied gas flows [27–34].

ENS models attempt to include the nonequilibrium effects from different viewpoints. An interesting approach is to revise the Navier-Stokes constitutive relationship with an effective viscosity to account for the information of the KL. For instance, based on elementary kinetic theory Li *et al.* [29] proposed an effective viscosity to account for the wall effect in a wall-adjacent layer ($y < \lambda$ with y being the distance to the wall). Alternatively, Lockerby *et al.* [31] introduced the concept of wall function into a scaled stress or strain rate constitution relation by fitting the velocity profile obtained from the linearized Boltzmann equation for the Kramers' problem. This idea was further extended and several new wall functions were developed (e.g., Refs. [30,33]). Usually these wall functions are continuous in terms of the distance to the wall. On the other hand, Lilley and Sader [35] proposed a discontinuous correction function by considering the separate velocity profiles of the Karmer's problem in the near-wall ($y < \lambda$) and far-wall ($y > \lambda$) regions. It is noted that this model is applicable only to fully diffuse walls, and the model parameters were determined by fitting the velocity profile of the Kramer's problem to the numerical solutions of the Boltzmann equation. A discontinuous correction function that can be applied to partially diffuse walls was developed [36] in which the molecular collisions in the near wall at $y > \lambda/2$ and $y \leqslant \lambda/2$ are considered separately. The ENS models usually contain some empirical parameters, and Guo *et al.* [28] developed an ENS model without free parameters based on the concept of effective mean-free path in which the wall confinement effect is considered. The model was shown to be able to give reasonable results in comparison with the DSMC data [37] and was further simplified with some numerics recently [38]. Unlike the model [28] where the molecular free path is assumed to follow an exponential distribution, Dongari *et al.* [39] assume that the molecular free path follows a power distribution and proposed an alternative wall function

for flat walls [40], which was further generalized to circular cylinders [41].

Although these ENS models have been demonstrated to be able to capture the critical behaviors within the KL and can improve predictions over a wider range of Kn, most previous studies were based on slip boundary conditions for the classical Navier-Stokes equations except for very few works. As far as the authors know, the first boundary condition for ENS models is due to Lockerby *et al.* [31], who suggested a first-order slip boundary condition by replacing the mean-free path with the effective one in the Maxwell slip boundary condition (1). Two second-order microslip boundary conditions for ENS models were also developed [28,30] but are limited to fully diffuse flat walls. Therefore, it is still an open problem to specify a suitable boundary condition for the extended Navier-Stokes equations in general cases. The present work aims to fill this gap, and the rest of this paper is organized as follows. A heuristic second-order slip boundary condition for the ENS is proposed in Sec. II, then some numerical results with the ENS coupled with the slip boundary condition are provided in Sec. III, and a brief summary is presented in Sec. IV.

II. A GENERALIZED SLIP BOUNDARY CONDITION

In ENS models, the generalized Navier-Stokes constitution can be expressed as

$$\boldsymbol{\tau}_e = \mu_e \dot{\boldsymbol{\gamma}}, \tag{2}$$

where $\boldsymbol{\tau}_e$ is the effective shear stress, $\dot{\boldsymbol{\gamma}} = \nabla \boldsymbol{u} + (\nabla \boldsymbol{u})^T - \frac{2}{3}(\nabla \cdot \boldsymbol{u})\boldsymbol{I}$ is the shear-strain rate (here $\boldsymbol{u}$ is the fluid velocity and $\boldsymbol{I}$ is the idendity tensor), and μ_e is an effective viscosity relating to the normal constant viscosity μ in the bulk region:

$$\mu_e(\boldsymbol{r}) = \mu\psi(\boldsymbol{r}), \tag{3}$$

where the function ψ, which is termed "correction function" in this work, depends on the local position $\boldsymbol{r}$. A number of correction functions have been proposed from different viewpoints, as mentioned in the introduction. But it should be emphasized that most of the available correction functions, except that in Ref. [41], are all designed for planar walls. Generally it is rather difficult to define such a function for a surface with irregular geometries. But in cases of the local curvature of the surface is small, the correction function can be employed as an approximation to the real one. In Table I some expressions of the correction function for flat walls are listed. With the extended Navier-Stokes constitution, the governing equations for an incompressible flow can be expressed as

$$\nabla \cdot \boldsymbol{u} = 0, \tag{4a}$$

$$\rho \left(\partial_t \boldsymbol{u} + \boldsymbol{u} \cdot \nabla \boldsymbol{u}\right) = -\nabla p + \nabla \cdot \boldsymbol{\tau}_e, \tag{4b}$$

where ρ, $\boldsymbol{u}$, and p are the fluid density, velocity, and pressure, respectively.

Now we discuss boundary conditions for the ENS (4). First we consider the case of flat walls, which is easy to illustrate the basic idea. As sketched in Fig. 1, outside the KL the velocity profile predicted by the classical Navier-Stokes equations can match the actual one provided a proper slip boundary condition is employed. But within the KL, they may differ from each other greatly. Consequently the microscopic velocity at the

TABLE I. Correction functions for planar walls; y is the distance to the wall, and $\hat{y} = y/\lambda$.

Reference	Acronym	Correction function $\psi(y)$
Lockerby et al. [31]	LRG	$[1 + C(1 + \hat{y}^3)^{-1}]^{-1}, \ C \approx 0.7$
Lilley and Sader [35]	LS	$\begin{cases} \alpha C \hat{y}^{1-\alpha}, & \hat{y} \leqslant 1 \\ 1, & \hat{y} > 1. \end{cases} \quad [(\alpha, C) \approx (0.8, 1.24)]$
Lockerby and Reese [30]	LR	$[1 + \phi_1(\hat{y}) + k\phi_2(\hat{y})]^{-1}, k = \dfrac{1}{\tau}\dfrac{d\tau}{d\hat{y}}$
		$\phi_i(y) = a_i \hat{y}^{b_i} \exp(c_i \hat{y}) \quad (i = 1, 2),$
		$(a_1, b_1, c_1) \approx (0.1859, -0.4640, -0.7902),$
		$(a_2, b_2, c_2) \approx (0.4205, -0.3518, -0.4521)$
Li et al. [29]	LWP	$1 - 0.5e^{-C\hat{y}}, C \approx 1.35$
Fichman and Hetsroni [36]	FH	$\begin{cases} \frac{\sigma}{2} + (1 - \sigma)\hat{y}, & \hat{y} \leqslant 1 \\ 1, & \hat{y} > 1. \end{cases}$
Reese et al. [33]	RZL	$\left[1 - A(D\sigma + E)(1 + \hat{y})^{A-1}\right]^{-1}$
		$(A, D, E) \approx (-2.719, -0.293, 0.531)$ for BGK
		$(A, D, E) \approx (-2.025, -0.328, 0.612)$ for hard sphere
Guo et al. [28]	GSZ	$1 + 0.5[(\hat{y} - 1)e^{-\hat{y}} - \hat{y}^2 E_i(\hat{y})],$
		$E_i(x) = \int_1^\infty t^{-1} e^{-xt} \, dt$
Dongari et al. [40]	DZR	$1 - \frac{1}{96}\left[\left(1 + \frac{\hat{y}}{a}\right)^{1-n} + 4\sum_{i=1}^{8}\left(1 + \frac{\hat{y}}{a\cos[(2i-1)\pi/32]}\right)^{1-n}\right.$
		$\left. + 2\sum_{i=1}^{7}\left(1 + \frac{\hat{y}}{a\cos[i\pi/16]}\right)^{1-n}\right], \quad a = n - 2$

wall, u_s, is usually different from the apparent macroscopic slip velocity, u_s^{ns}, that is extrapolated from the Navier-Stokes solution in the bulk region.

A number of slip boundary conditions for the macroscopic slip velocity u_s^{ns} have been proposed in the literature. Besides Maxwell's first-order slip boundary condition given by Eq. (1), some second-order boundary conditions were also suggested from different viewpoints. In general a second-order slip boundary condition for a flat wall can be written as

$$u_s^{ns} = A_1^{ns} \lambda \partial_{\boldsymbol{n}} u - A_2^{ns} \lambda^2 \partial_{\boldsymbol{n}}^2 u, \tag{5}$$

where A_1^{ns} and A_2^{ns} are the first- and second-order slip coefficients, respectively, and both depend on the gas-wall interactions. These coefficients can be obtained either by experiments or by kinetic theory, and a thorough discussion about slip boundary conditions has been conducted recently by Hadjiconstantinou [42].

On the other hand, the knowledge about the microscopic velocity u_s is rather limited. Based on a variational method, Cercignani [1] solved the linearized Boltzmann BGK equation for the Kramers' problem with a fully diffuse flat wall and found that

$$u_s = \frac{\sqrt{\pi}}{2}\lambda\frac{\tau}{\mu} = \frac{\sqrt{\pi}}{2}\lambda\partial_{\boldsymbol{n}} u, \tag{6}$$

where τ is the applied tangential shear stress parallel to the wall in the Kramers' problem. Furthermore, Loyalka et al. [11] shown that for a flat wall with accommodation coefficient σ, the microslip velocity in the Kramers' problem is

$$u_s \approx \frac{2 - \sigma}{\sigma}(1 - 0.1817\sigma)\lambda\frac{\tau}{\mu} = \frac{2 - \sigma}{\sigma}(1 - 0.1817\sigma)\lambda\partial_{\boldsymbol{n}} u. \tag{7}$$

As $\sigma = 1$, i.e., the wall is fully diffusive, u_s given by this equation is in good agreement with the exact solutions of the linearized BGK equation [1].

Motivated by Eqs. (5) and (7), we propose a heuristic second-order slip boundary condition for the microscopic slip velocity u_s:

$$u_s = A_1 \lambda_e \partial_{\boldsymbol{n}} u - A_2 \lambda_e \partial_{\boldsymbol{n}}(\lambda_e \partial_{\boldsymbol{n}} u), \tag{8}$$

where the two slip coefficients are assumed to be

$$A_1 = \frac{2 - \sigma}{\sigma}(1 - 0.1817\sigma), \quad A_2 = \sigma^2\left[\frac{1}{\pi} + \frac{1}{2}A_1^2\right]. \tag{9}$$

Here the relation between the first and second-order slip coefficients is motivated by that for the macroscopic slip velocity: According to Cercignani's result of the Boltzmann equation for the Poiseuille flow with two fully diffuse walls [1], the two slip coefficients are $A_1^{ns} = 2\zeta/\sqrt{\pi}$ and $A_2^{ns} = \pi^{-1} + (A_1^{ns})^2/2$, with $\zeta = 1.016$. Equation (9) is just a generalization of this relationship. λ_e in the proposed boundary condition (8) is an effective mean-free path depending on the correction function, $\lambda_e/\lambda = \mu_e/\mu = \psi$, which can be viewed as a generalization of the relation between the mean-free path and the viscosity [1]:

$$\lambda = \frac{\mu}{p}\sqrt{\frac{\pi R T}{2}}. \tag{10}$$

Now we generalize the second-order slip boundary condition (8) to the case of curved surfaces. For a curved wall, the slip velocity is given by

$$u_s = A_1 \lambda_e \dot{\gamma}_{r\theta} - A_2 \lambda_e r^n \partial_{\boldsymbol{n}}\left(\frac{1}{r^n}\lambda_e \dot{\gamma}_{r\theta}\right), \tag{11}$$

where u_s is now the slip velocity tangential to the surface, r is the local radius of the curvature of the surface (positive for concave and negative for concave), θ is the polar angle, and $\dot{\gamma}_{r\theta}$ is the radial-tangential component of the strain rate on the surface. The parameter n depends on the local coordinates: $n = 0$, 1, and 2 for the Cartesian, cylindrical, and spherical coordinate systems respectively. The two slip coefficients A_1 and A_2 are still specified according to Eq. (9). It can be easily shown that in the limit of flat wall ($r \rightarrow \infty$), the curved boundary condition (11) reduces to Eq. (8), indicating the consistency of the generalization.

It should be noted that λ_e in the proposed boundary condition (8) and (11) is a local variable. Particularly, as λ_e takes a constant value, Eq. (8) takes the same formulation as the standard second-order slip boundary condition (5) for the classical Navier-Stokes equations. Generally the use of this local effective-mean-free path makes the slip velocity given by Eq. (8) smaller than that of the classical one given by Eq. (5), which is reasonable since the microslip velocity u_s is usually smaller than the extrapolated Navier-Stokes slip velocity u_s^{ns}. Another point about the proposed boundary condition that should be emphasized is that the effective mean-free path is included within the second derivative rather than outside it, unlike the conventional second-order boundary conditions. Such a choice is consistent with the philosophy of Maxwell's argument on slip boundary conditions; i.e., the slip should be expressed in terms of stress rather than strain rate, as revisited in Ref. [3].

It is interesting to note that a slip boundary condition similar to the present one was suggested in Ref. [30] for fully diffuse walls, which can be expressed in the present nomenclature as

$$u_s = A_1 \lambda \frac{\tau}{\mu} - A_2 \frac{\lambda^2}{\mu} \frac{\partial \tau}{\partial \boldsymbol{n}} = A_1 \lambda_e \partial_{\boldsymbol{n}} u - A_2 \lambda \partial_{\boldsymbol{n}} \left(\lambda_e \partial_{\boldsymbol{n}} u \right),$$

(12)

where the relation $\tau/\mu = \psi \partial_{\boldsymbol{n}} u$ has been used, and the two slip coefficients $A_1 = 0.798$ and $A_2 = 0.278$ were determined by fitting to the low-Kn BGK solutions of the Couette and Poiseuille flows. It is obvious that this formulation is very similar to the present one as $\sigma = 1$; the difference lies in the mean-free path appearing in the second-order slip terms: one of the two λ_e is replaced by λ in Eq. (12). Despite this difference, both slip boundary conditions share one feature: they are expressed in terms of stress rather than strain rate, which is consistent with the analysis of Ref. [3].

III. RESULTS AND DISCUSSION

To test the performance of the proposed second-order slip boundary condition, in this section we will apply Eqs. (8) or (11) to several nonequilibrium flows involving flat or curved walls, and compare the solutions to some existing data by other methods.

A. Knudsen layer structure

The structure of the Knudsen layer can be studied using the Kramers' problem. This problem can serve as a good benchmark for testing new hydrodynamic models and boundary conditions due to its simplicity and available data from

kinetic theory or DSMC. For this problem the ENS model with the effective viscosity reduces to

$$\partial_y(\mu_e \partial_y u) = 0,$$

(13)

together with the second-order slip boundary

$$u = A_1 \lambda_e \partial_y u - A_2 \lambda_e \partial_y (\lambda_e \partial_y u)$$

(14)

at $y = 0$, and

$$\partial_y u = a = \text{const}$$

(15)

at $y = \infty$.

From Eq. (13) we can conclude that $\mu_e \partial_y u$ is a constant in the whole domain, and so is $\lambda_e \partial_y u$. Therefore, the second-order slip boundary condition actually acts as a first-order one for this problem. After some simple algebra we can obtain the velocity of the Kramers' problem,

$$u(y) = u_0 + a \int_0^y \psi^{-1}(y)\,dy,$$

(16)

where $u_0 = A_1 \lambda$ is the velocity at the wall. A numerical solution can then be obtained by discretizing Eq. (16):

$$u_{j+1} = u_j + a \int_{y_j}^{y_{j+1}} \psi^{-1}(y)\,dy, \quad j = 0, 1, \ldots, N.$$

(17)

where $y_j = j\Delta y$, and the trapezoidal rule is used to evaluate the integral with a mesh spacing $\Delta y = H/N$ in the interval $[0, H]$ with $H = 25\lambda$, and here $N = 2000$ is used which can give grid-independent solutions.

In Fig. 2 the velocity profiles near the wall predicted by the ENS model with different correction functions are shown, together with the solution of the linearized Boltzmann equation [14]. It is noted that for this problem the applied shear stress τ is constant, and so $k = 0$ in the model in Ref. [30]. As can be seen, the results of the ENS model with the correction function given by Ref. [35] deviate from the Boltzmann solutions significantly in both cases, while those with other correction functions are all rather satisfactory. These results suggest that the correction function [35], which is linear in the KL, is inadequate for capturing the structure of the KL, while the other nonlinear ones can help to predict the nonequilibrium flows within the KL in the Navier-Stokes framework. In what follows, we will consider only the correction function proposed in Ref. [28] for flows over flat walls unless stated otherwise, since it has a solid foundation and contains no empirical coefficients.

B. Planar Poiseuille flow

The proposed second-order slip boundary condition reduces to a first-order one in the Kramers' problem. To further demonstrate the applicability of this boundary condition, we now apply it to the plane Poiseuille flow driven by a constant force $\boldsymbol{a} = (a, 0)$, which exhibits a nonlinear velocity profile over the whole domain. The two parallel walls of the channel are assumed to be located at $y = 0$ and $y = h$, respectively. Note that for this problem the motion of gas molecules will be influenced by both walls, and the correction function should be modified to $\tilde{\psi}(y) = [\psi(y) + \psi(H - y)]/2$ since each molecule can move towards the two walls with the same probability [28]. Specifically, with the correction function
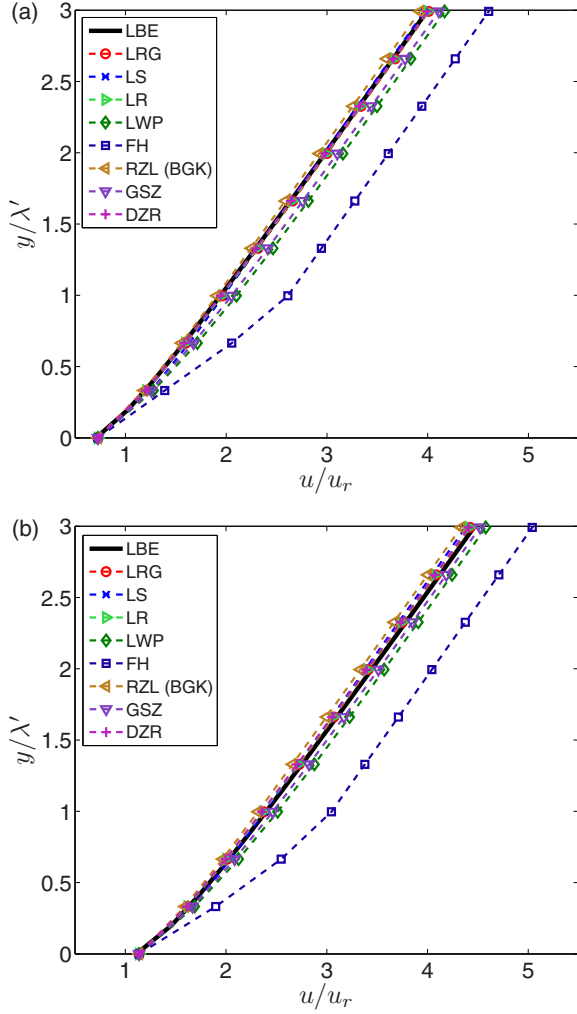
FIG. 2. (Color online) Velocity profiles of the Kramers' problem with different correction functions as well as the linearized Boltzmann equation (LBE) solution [14] under different accommodation coefficients. Here $\lambda' = (2/\sqrt{\pi})\lambda$ and $u_r = a\lambda'$. (a) $\sigma = 1.0$; (b) $\sigma = 0.8$.

given in Ref. [28], the expression is

$$\tilde{\psi}(y) = 1 + \left[(\hat{y} - 1)e^{-\hat{y}} + (\hat{y}_1 - 1)e^{-\hat{y}_1} - \hat{y}^2 E_i(\hat{y}) - \hat{y}_1^2 E_i(\hat{y}_1) \right], \quad (18)$$

where $\hat{y}_1 = (H - y)/\lambda$, and $E_i(x)$ is the exponential integral function as given in Table I.

For the planar Poiseuille flow the ENS model (4) reduces to the following equation for the streamwise velocity u:

$$\partial_y(\mu_e \partial_y u) + \rho a = 0, \quad (19)$$

where ρ is the gas density and is assumed to be a constant. The boundary conditions at the bottom and top walls are

$$u_0 = A_1^b \lambda_e \partial_y u - A_2^b \lambda_e \partial_y(\lambda_e \partial_y u) \quad (y = 0), \quad (20a)$$

$$u_h = -A_1^t \lambda_e \partial_y u - A_2^t \lambda_e \partial_y(\lambda_e \partial_y u) \quad (y = h), \quad (20b)$$

where A_i^t and A_i^b $(i = 1, 2)$ are the slip coefficients for the top and bottom walls, respectively, which depend on the accommodation coefficients of the two walls (σ_t and σ_b). With

these boundary conditions, we can find the solution of Eq. (19),

$$u(y) = u_0 - \rho a \int_0^y y \mu_e^{-1}(y)\,dy + c_0 \int_0^y \mu_e^{-1}(y)\,dy, \quad (21)$$

where

$$\begin{aligned} u_0 &= \frac{A_1^b c_0 + A_2^b \lambda_e(0)\rho a}{\alpha}, \\ c_0 &= \frac{\alpha K_1 + A_1^t h + A_2^t \lambda_e(h) - A_2^b \lambda_e(0)}{\alpha K_0 + A_1^t + A_1^b} \rho a \end{aligned} \quad (22)$$

with $\alpha = \mu_e/\lambda_e = \rho(2RT/\pi)^{1/2}$, and

$$K_0 = \int_0^h \mu_e^{-1}(y)\,dy, \quad K_1 = \int_0^h y \mu_e^{-1}(y)\,dy. \quad (23)$$

The velocity is then obtained numerically from Eq. (21),

$$u_{j+1} = u_j - \rho a \int_{y_j}^{y_{j+1}} y \mu_e^{-1}(y)\,dy + c_0 \int_{y_j}^{y_{j+1}} \mu_e^{-1}(y)\,dy, \quad (24)$$

where the trapezoidal rule is used to evaluate the two integrals again. Here 2000 grid points are employed, which is good enough to obtain the grid-independent results.

First, we consider the case of fully diffuse walls ($\sigma_t = \sigma_b = 1.0$). The normalized velocity profiles at several reduced Knudsen numbers $k = (\sqrt{\pi}/2)$Kn, with Kn defined by Kn $= \lambda/h$, are shown in Fig. 3, together with the solution of the Boltzmann equation [15]. For comparison, the solutions of the standard Navier-Stokes equations with two classical second-order slip boundary conditions are also presented. The first boundary condition uses the slip coefficients suggested previously [1], $A_1 = 1.1466$ and $A_2 = 0.9795$, while the second one uses the improved version proposed in Ref. [42] which considers the Knudsen layer effects, $A_1 = 1.11$ and $A_2 = 0.31$. For brevity we will denote the former and latter as "NS-C" and "NS-H," respectively. The results of the ENS with the second-order microslip boundary condition previously proposed in Ref. [30] [see Eq. (12)], denoted by "ENS-LR," are also included in the figure.

It is observed that as $k = 0.1$, the velocity profiles predicted by the four methods, which are normalized by $u_r = ah\sqrt{2/RT}$, are all in good agreement with the solution of the linearized Boltzmann equation [15], except that the NS-C over predicts slightly; it is also clearly seen that both the present method and the ENS-LR give better predictions in the KLs near the two walls. As k increases to 0.4, the NS-C gives an obvious overestimation; The profiles of the present method and the NSE-H are nearly identical in the central region, but the former is much better in the KLs; The profile of the ENS-LR is also satisfactory in the KLs, almost overlaps that of the present method, but the deviation from the linearized Boltzmann solution is slightly larger than that of the present method.

As k increases to 1.0, the NS-C fails to capture the basic feature of the flow; the NS-H gives a better prediction but still shows some obvious derivations. On the other hand, both the ENS together with the proposed boundary condition and the ENS-LR yield much better solutions. As k goes up to 8.0, both NS-C and NS-H fail to give satisfactory results, which is
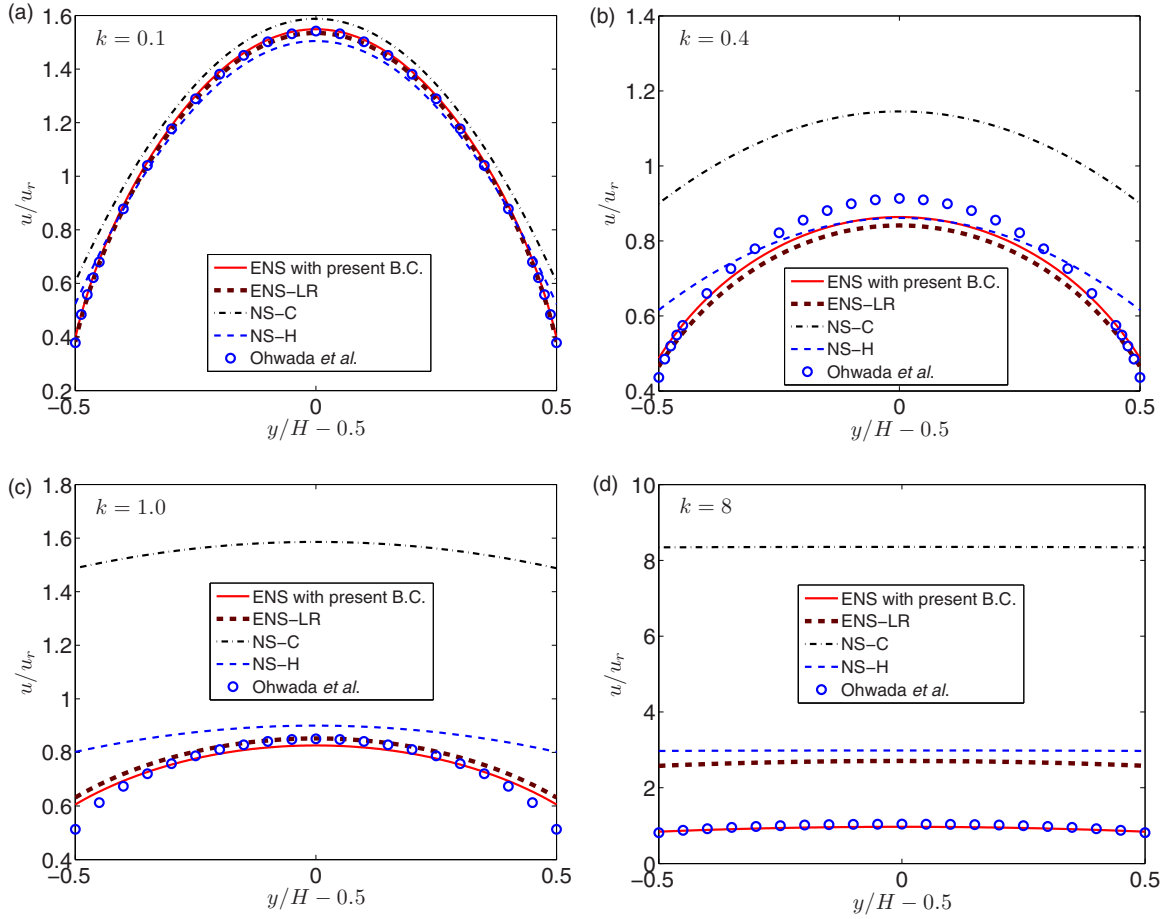
FIG. 3. (Color online) Velocity profiles of the Poiseuille flow ($k = (\sqrt{\pi}/2)$Kn, Kn $= \lambda/h$, and $u_r = ah/\sqrt{2/RT}$) predicted by the Navier-Stokes and extended Navier-Stokes models coupled with different boundary conditions. The solution of the linearized Boltzmann equation are from Ref. [15].

not surprising since the classical Navier-Stokes model breaks down completely under such high Knudsen numbers; the ENS-LR gives a slightly better prediction than the NS-H, but the departure of the result from the reference solution is significant. On the other hand, the result of the present method is still in good agreement with the solution of linearized Boltzmann equation.

The dimensionless mass fluxes, $Q = (\rho u_r h)^{-1} \int_0^h \rho u(y) dy$, computed from the four models and the classical Navier-Stokes equation with no-slip boundary conditions, are shown in Fig. 4. It is seen that all of the three slip models are able to give accurate mass fluxes as $k \leqslant 0.1$ in comparison with the solutions of the Boltzmann equation [15]. As k becomes larger, the NS-C fails to work anymore, but the NS-H can works well up to $k \approx 0.3$, which is consistent with the analysis in Ref. [42]. The ENS-LR can give good predictions up to $k = 1.0$, which is not surprising since the LR boundary condition is obtained by fitting the model to the low-Kn Couette and Poiseuille flows [30]. On the other hand, the present model yields satisfied results in a rather larger region (up to about $k = 10$), and the Knudsen minimum is captured successfully.

Now we consider flows with two identical partial diffuse walls ($\sigma_b = \sigma_t = \sigma < 1.0$). Note that the LR boundary con-

dition cannot be used in this case since it is designed for fully diffuse walls. Because of the lack of data for the velocity profile
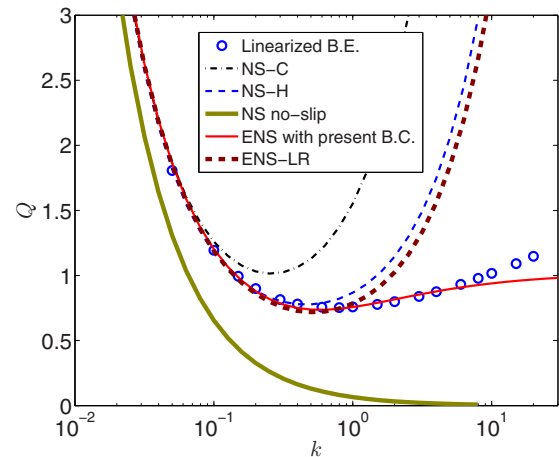

FIG. 4. (Color online) Normalized mass flux of the planar Poiseuille flow with fully diffusive walls predicted by the Navier-Stokes and extended Navier-Stokes models coupled with different boundary conditions. The solution of the linearized Boltzmann equation (open circles) is taken from Ref. [15].
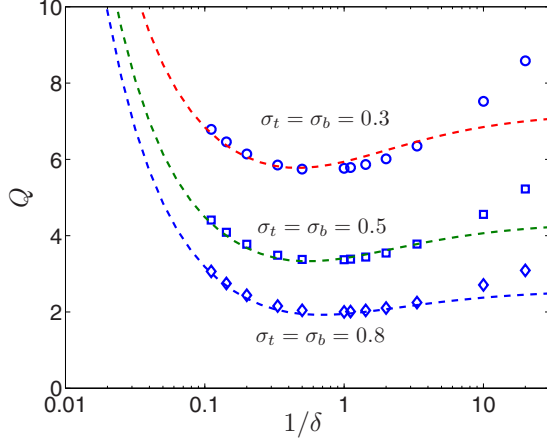
FIG. 5. (Color online) Normalized mass flux of the planar Poiseuille flow with partially diffusive walls. Symbols: solutions of the linearized Boltzmann equation taken from Ref. [43]; lines: solutions of the present ENS with the proposed slip boundary condition

in the literature, here we show only the normalized mass fluxes (Fig. 5). For comparison we use the notations of Ref. [43], e.g., the inverse Knudsen number $\delta = (\sqrt{\pi}/2)\mathrm{Kn}^{-1}$ and the mass flux Q normalized by $\rho a h^2/\sqrt{2RT}$. As shown, the mass fluxes with different accommodation coefficients predicted by the present method are in good agreement with the solutions of the linearized Boltzmann equation [43] as δ^{-1} is below 10, and the Knudsen minimums are all captured successfully.

Flows with nonidentical walls are also considered. Figure 6 shows the normalized mass fluxes with different values of σ_t and $\sigma_b = 1.0$. Good agreement between the predictions of the present method and the results of the LBE [43] is again observed.

C. Microcylindrical Couette flow

In the above test problems only planar walls are involved. In order to further validate the capability of the proposed method, now we consider the cylindrical Couette flow between two concentric cylinders (with radius R_1 and R_2 respectively),
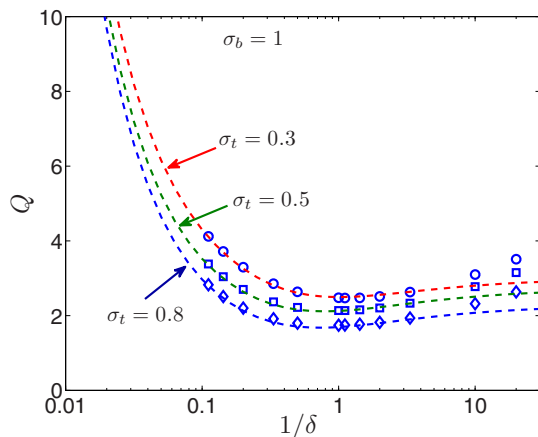

FIG. 6. (Color online) Same as in Fig. 5 except with $\sigma_b = 1$ and variable σ_t.

which is a well-known classical fluid-dynamics problem. Although the geometry is simple, some recent studies show that this flow exhibits some nonintuitive behaviors as slip occurs at the cylinder surfaces. An example is the occurrence of "velocity inversion" phenomenon, which has been studied based on different approaches (see Ref. [44] and references therein). For this problem the extended Navier-Stokes equation in the polar coordinates (r, θ) can be expressed as

$$\frac{1}{r^2}\frac{d}{dr}(\mu_e r^2 \dot{\gamma}_{r\theta}) = 0 \tag{25}$$

where u is the tangential velocity, and $\dot{\gamma}_{r\theta}$ is the tangential shear rate:

$$\dot{\gamma}_{r\theta} = \frac{du}{dr} - \frac{u}{r} = r\frac{d}{dr}\left(\frac{u}{r}\right). \tag{26}$$

The solution of Eq. (25) is

$$\frac{u}{r} = c_0 \int_{R_1}^{r} \frac{1}{\mu_e r^3}\, dr + \frac{u_1}{R_1}, \tag{27}$$

where c_0 is a constant and u_1 is the tangential slip velocity at the surface of the inner cylinder. Both c_0 and u_1 depend on the boundary conditions at the cylinder surfaces. In this case the slip boundary conditions on the inner and outer cylinders based on Eq. (11) can be expressed as

$$
\begin{aligned}
u_s(R_1) &\equiv u(R_1) - \omega_1 R_1 \\
&= A_1^i\, [\lambda_e \dot{\gamma}_{r\theta}]|_{r=R_1} - A_2^i \left[\lambda_e r\frac{d}{dr}\left(\frac{1}{r}\lambda_e\dot{\gamma}_{r\theta}\right)\right]\Big|_{r=R_1},
\end{aligned}
\tag{28a}
$$

$$
\begin{aligned}
u_s(R_2) &\equiv u(R_2) - \omega_2 R_2 \\
&= -A_1^o\, [\lambda_e \dot{\gamma}_{r\theta}]|_{r=R_2} - A_2^o \left[\lambda_e r\frac{d}{dr}\left(\frac{1}{r}\lambda_e\dot{\gamma}_{r\theta}\right)\right]\Big|_{r=R_2},
\end{aligned}
\tag{28b}
$$

where A_k^i and A_k^o ($k = 1,2$) are the slip coefficients of the inner and outer cylinder surfaces which are associated with the accommodation coefficients σ_i and σ_o through Eq. (9), respectively, and ω_1 and ω_2 are the rotating angular velocities of the inner and outer cylinders, respectively.

With the above boundary conditions, it can be shown that

$$c_0 = -\frac{\omega_1 - \omega_2}{K}, \quad u_1 = \omega_1 R_1 + B_1\frac{c_0}{\alpha R_1^2}, \tag{29}$$

where

$$K = \int_{R_2}^{R_2} \frac{1}{\mu_e r^3}\, dr + \frac{1}{\alpha}\left(\frac{B_1}{R_1^3} + \frac{B_2}{R_2^3}\right) \tag{30}$$

with $\alpha = \mu_e/\lambda_e$, and

$$B_1 = A_1^i + 3A_2^i\frac{\lambda_e(R_1)}{R_1}, \quad B_2 = A_1^o - 3A_2^o\frac{\lambda_e(R_2)}{R_2}. \tag{31}$$

Once c_0 and u_1 are determined, the velocity u can be obtained numerically from Eq. (27). Here we used a grid with a resolution of $\Delta r = |R_1 - R_2|/2000$, which is enough to obtain grid-independent solutions.

It is noted that if the following classical first-order slip boundary condition is used:

$$u_s^i = \frac{2 - \sigma_i}{\sigma_i} \lambda \dot{\gamma}_{r\theta} \Big|_{r=R_1}, \quad u_s^o = -\frac{2 - \sigma_o}{\sigma_o} \lambda \dot{\gamma}_{r\theta} \Big|_{r=R_2}, \quad (32)$$

the solution of the original Navier-Stokes equations with a constant viscosity is [44]

$$\frac{u}{\omega_1 R_1} = \frac{1}{(A - B)R_1} \left(Ar - \frac{1}{r} \right), \quad (33)$$

where

$$A = \frac{1}{R_2^2} \left(1 - 2 \frac{2 - \sigma_o}{\sigma_o} \frac{\lambda}{R_2} \right), \quad B = \frac{1}{R_1^2} \left(1 - 2 \frac{2 - \sigma_i}{\sigma_i} \frac{\lambda}{R_1} \right). \quad (34)$$

We consider the case when both cylinders have an identical accommodation coefficient ($\sigma_i = \sigma_o = \sigma$), which was also investigated by DSMC and lattice Boltzmann equation methods [44,45]. The radius of the cylinders are chosen to be $R_1 = 3\lambda$ and $R_2 = 5\lambda$, and the outer cylinder is fixed while the inner one rotates with $\omega_i = \omega$. The velocity profiles of this flow with different values of σ are shown in Fig. 7, together with the DSMC data [45] and the solutions of the standard Navier-Stokes model given by Eq. (33). It is clearly seen that the fundamental behaviors of the flow are successfully
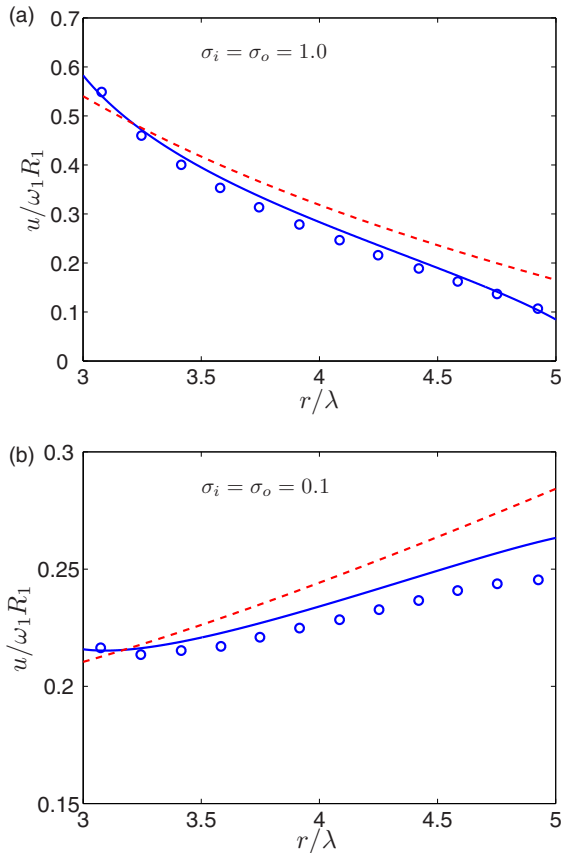

(a)

(b)

FIG. 7. (Color online) Velocity profiles of the cylindrical Couette flow. Open circle: DSMC data from Ref. [45]; Solid line: ENS with present slip boundary condition; dashed line: Navier-Stokes with classical first-order slip boundary condition.

captured in comparison with the DSMC results. In particular, the velocity inversion is observed as $\sigma = 0.1$. It is also noted that the present method yields more accurate predictions than the standard Navier-Stokes equation with the usual slip boundary conditions in comparison with the DSMC results. We would like to note here that recently a similar study on this problem was also conducted by Dongari *et al.* [41], where a power-law correction function together with a first-order slip boundary condition was employed.

D. Low speed flow over a microsphere

To further validate the proposed method, we also considered the low-speed gas flow over a sphere with radius R. The gas is assumed to be incompressible and obeys the Stokes equations with the extended viscosity:

$$\nabla \cdot \boldsymbol{u} = 0, \quad \nabla \cdot \boldsymbol{\tau}_e - \nabla p = 0. \quad (35)$$

As shown previously [46], in spherical coordinate (r, θ, ϕ) with the origin at the sphere center, the flow velocity $\boldsymbol{u} = (u_r, u_\theta, u_\phi)$ can be related to a scalar variable f:

$$u_r = \frac{2\beta f}{r} \cos\theta, \quad u_\theta = -\beta \left(\frac{df}{dr} + \frac{f}{r} \right) \sin\theta, \quad (36)$$

where $\beta = (3/8\pi)^{1/2}$. The variable f only depends on r and satisfies the following ordinary differential equation (ODE):

$$\mu_e \left(r^3 \frac{d^3 f}{dr^3} + r^2 \frac{d^2 f}{dr^2} - 6r \frac{df}{dr} + 6f \right)$$
$$+ \frac{d\mu_e}{dr} \left(r^3 \frac{d^2 f}{dr^2} \right) = K, \quad (37)$$

where K is a constant from which the drag force on the sphere can be determined:

$$F = -\frac{K}{2\beta}. \quad (38)$$

Some constraints on Eq. (37) for f can be obtained from the velocity boundary conditions. As $r \to \infty$, the velocity approaches to the free stream velocity u_∞, i.e., $u_r \to u_\infty \cos\theta$ and $u_\theta \to -u_\infty \sin\theta$, from which we can deduce that

$$\lim_{r\to\infty} \frac{f}{r} = \frac{u_\infty}{2\beta}, \quad \lim_{r\to\infty} \frac{df}{dr} = \frac{u_\infty}{2\beta}. \quad (39)$$

On the other hand, at the surface of the sphere ($r = R$) we must have $u_r = 0$, and u_θ is assumed to satisfy the proposed second-order slip boundary condition,

$$u_\theta = A_1 \lambda_e \dot{\gamma}_{r\theta} F - A_2 \lambda_e r^2 \frac{\partial}{\partial r} \left(\frac{1}{r^2} \lambda_e \dot{\gamma}_{r\theta} \right), \quad (40)$$

where

$$\dot{\gamma}_{r\theta} = \frac{\partial u_\theta}{\partial r} + \frac{1}{r} \frac{\partial u_r}{\partial \theta} - \frac{u_\theta}{r} = -\beta \frac{d^2 f}{dr^2} \sin\theta. \quad (41)$$

Therefore, at $r = R$ the function f must satisfy

$$f = 0, \quad \frac{df}{dr} = A_1 \lambda_e \frac{d^2 f}{dr^2} - A_2 r^2 \lambda_e \frac{d}{dr} \left(\frac{\lambda_e}{r^2} \frac{d^2 f}{dr^2} \right). \quad (42)$$

With the constraints given by Eqs. (39) and (42), the ODE (37) together with the parameter K can be solved numerically.
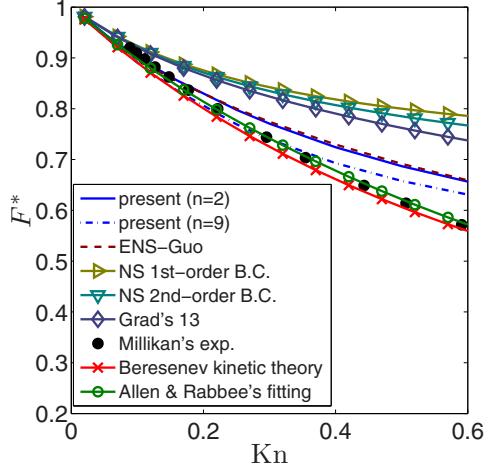
FIG. 8. (Color online) Drag force over a sphere predicted by the Navier-Stokes and extended Navier-Stokes models coupled with different boundary conditions. The experimental data [51], the fitting curve (47), and the kinetic theory result are presented as well for comparison.

In our simulations the computational domain is set to be $[R, 1000R]$, and the ODE is solved via the standard MATLAB function bvp4c, which is an efficient self-adaptive solver for general boundary value problems of ODE [47]. In Fig. 8 the nondimensional drag force, $F^* = F/(6\pi\mu R u_\infty)$, is shown as a function of the Knudsen number $\mathrm{Kn} = \lambda/R$. Here the sphere is assumed to be fully diffusive ($\sigma = 1.0$). For comparison, we also show in the figure some other results reported in the literature, including the Navier-Stokes solution with the classical first-order slip boundary condition,

$$F^* = \frac{1 + 2C\mathrm{Kn}}{1 + 3C\mathrm{Kn}}, \qquad (43)$$

where $C = (2 - \sigma)/\sigma$, and that with a second-order slip boundary condition [48],

$$F^* = \frac{1 + 2\mathrm{Kn}}{1 + 3C\mathrm{Kn} + [(9/4\pi)(\gamma - 1)/\gamma]\mathrm{Pr}\mathrm{Kn}^2}, \qquad (44)$$

where Pr is the Prandtl number and γ is the ratio of specific heat capacities. Here we consider a monatomic gas, i.e., $\mathrm{Pr} = 2/3$ and $\gamma = 5/3$. Also included is the solution of Grad's 13 moment equations [49],

$$F^* = \frac{(1 + 2\mathrm{Kn})(1 + 7.5C\mathrm{Kn}) + (\pi/6)\mathrm{Kn}^2}{(1 + 3C\mathrm{Kn})(1 + 7.5C\mathrm{Kn}) + (9/5\pi)(4 + 9C\mathrm{Kn})\mathrm{Kn}^2}, \qquad (45)$$

and the result derived from the kinetic theory [50],

$$F^* = \frac{8 + \pi}{18(0.619 + \mathrm{Kn})}\left(1 + \frac{0.31\mathrm{Kn}}{0.785 + 1.152\mathrm{Kn} + \mathrm{Kn}^2}\right), \qquad (46)$$

as well as experimental data [51] and fitting curve [52],

$$F^* = [1 + \mathrm{Kn}(1.142 + 0.558e^{-0.999/\mathrm{Kn}})]^{-1}. \qquad (47)$$

Most of these reference formulations can also be found in Ref. [48]. We also show the results of Ref. [28] in the figure

(denoted by "ENS-Guo") where the following slip boundary condition was employed:

$$u_\theta = A_1\lambda_e\partial_r u_\theta - A_2\lambda_e\partial_r(\lambda_e\partial_\theta u_\theta), \qquad (48)$$

with $A_1 = 1.0$ and $A_2 = 0.5$. This boundary condition is a direct extension of that for flat walls and the curvature effect is not considered, which is problematic for general curved walls [3]. Actually this boundary condition does not work well for the cylindrical Couette flow due to the absence of curvature effect. It is interesting that, however, the drag coefficients predicted by the ENS with this boundary condition are nearly the same as those with the present microslip boundary condition. From Fig. 8 it can also be observed that the results from kinetic theory agree well with the experimental data, while the predictions of the standard Navier-Stokes model with either the classical first-order or the second-order slip boundary conditions show great derivations except for rather small values of Kn ($\leqslant 0.1$); the solution of the Grad's 13 moment model gives some slight improvement, although it is still not satisfactory. On the other hand, the present
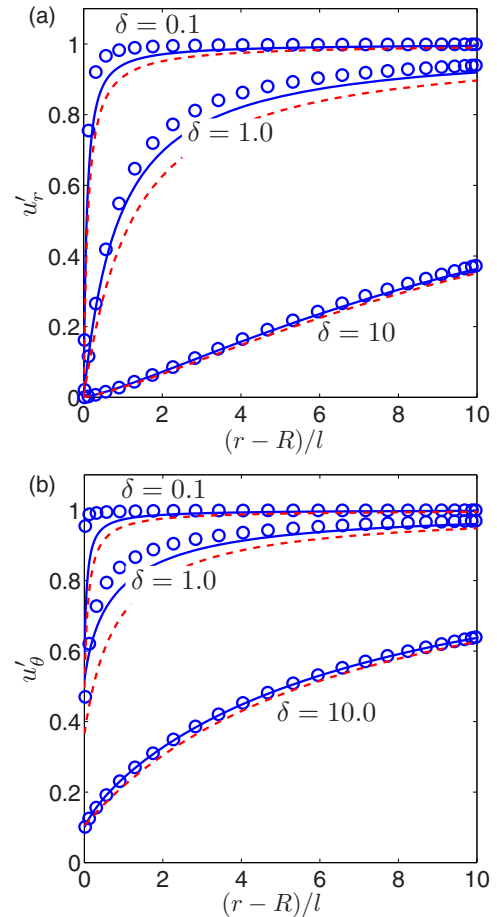

FIG. 9. (Color online) Velocity profiles at different Knudsen numbers. Here $l = (2/\sqrt{\pi})\lambda$, $u_r' = u_r/u_\infty \sin\theta$, and $u_\theta' = -u_\theta/u_\infty \cos\theta$. Open circles: solution of the linearized Boltzmann equation [53]; solid lines: solution of the extended Navier-Stokes model with present boundary condition; dashed lines: solution of the Navier-Stokes equations with first-order slip boundary condition [54].

method gives much improved predictions and is satisfactory as Kn $\leqslant 0.2$. It is also interesting that the prediction can be further improved if we treat the parameter n in the second-order slip term as an adjustable parameter. An example of $n = 9$ is shown in Fig. 8. It can be seen that with this choice the predicted drag coefficient agrees with the kinetic theory and experimental data up to Kn $= 0.4$. This may suggest that we may treat n as a free model parameter rather than a fixed one in applications. We also measured the velocity distributions from the computed values of f under different sphere radius. The two normalized components in three cases are shown in Fig. 9, where the solutions of the linearized Boltzmann equation [53] and the analytical solution of the Navier-Stokes equations with the classical slip boundary condition [54] are also included for comparison. It can be seen that as the inverse Knudsen mumber, $\delta = (\sqrt{\pi}/2)\mathrm{Kn}^{-1}$, is large ($\delta = 10.0$), the results of the three methods agree well with each other in whole region; as δ decreases to 1.0, both the present results and the Navier-Stokes solutions deviate form the kinetic solutions greatly, particularly the tangential component in the near-wall region. As δ goes further down to 0.1, the velocity deviations of both methods are more significant in the near-wall region, and the predictions of the tangential velocity component are even unacceptable in this case. However, it can also be observed that the present method can give better predictions than the classical Navier-Stokes with the slip boundary condition in all cases.

IV. SUMMARY

It is a changeling task to model rarefied nonequilibrium gas flows in the continuum framework. The difficulty lies mainly in the capturing of the flows in the Knudsen layer. Recently some extended Navier-Stokes models, in which the Knudsen layer effects are incorporated through an effective viscosity, have been developed. However, it is still an open problem about how to specify a suitable boundary condition for such models. In this work we first identified two types of slip velocities at the solid wall. One is the usual fictitious macroscopic slip velocity for the standard Navier-Stokes equations, which plays a key role for capturing the bulk flow, and the other is the microscopic slip velocity that describes the average molecular velocity at the wall. A generalized second-order slip boundary condition for this microscopic slip velocity was then developed, which can be used for the extended Navier-Stokes models.

Coupled with certain extended Navier-Stokes models, the proposed slip boundary condition has been applied to several rarefied gas flows involving planar and curved boundaries, including the Kramers' problem, the planar Poiseuille flow, the cylindrical Couette flow, and the flow over a sphere. It is shown that the fundamental flow behaviors of these flows can be successfully captured by the present method, which

suggests that the proposed boundary condition is a good and potential model for the extended Navier-Stokes equations in the description of rarefied gas flows. However, it should be noted that in the case of flow over a sphere, the improvements are still limited. This limitation presumably is not only related to the proposed slip boundary condition, but also is related to the adopted form of the extended Navier-Stokes equations that incorporates the effective mean-free path for simple planar gas systems and may not be accurate for complex flows.

Finally, we would like to emphasize how the present work differs from several related ones [28,30,40,41]. In Ref. [28] a scheme similar to Eq. (8) is presented, but the scheme is for fully diffuse flat walls, and the two slip coefficients ($A_1 = 1$, $A_2 = 0.5$) were taken from the classical second-order slip boundary conditions for macroslip velocities. With this scheme, the Poiseuille flow in a channel with fully diffuse walls was simulated, but no results were reported for cases of partial diffuse walls; the flow around a microsphere was also simulated with the boundary condition, but the curvature effect was not considered. The scheme used in Ref. [40] is the same as that in Ref. [28] except for $A_2 = 0.31$, which was taken from the macroscopic slip boundary condition proposed in Ref. [10]. With this scheme the Poiseuille flow in a channel was simulated where again only cases of fully diffuse walls were considered. In Ref. [41], the cylindrical Couette flow was investigated by solving an ENS model with a first-order slip boundary condition, where the slip coefficient A_1 was again set to be the same as that used in classical slip boundary conditions ($A_1 = (2 - \sigma)/\sigma$). It is interesting that the velocity inversion was also observed with this slip boundary condition. In Ref. [30] a slip boundary condition for fully diffuse walls was proposed in terms of stress rather than strain rate, just like the present scheme. The main difference lies in the second-order terms [refer to Eqs. (8) and (12)]: In the scheme of Ref. [30] both the mean-free path and the effective mean-free path are involved, while the present scheme uses only the effective one. Furthermore, the slip coefficients in these two schemes are also different. To summarize, the slip boundary condition in the present work is different from those used in the previous studies, and with this boundary condition the numerical results for some test problems are also different from those reported in Refs. [28,30,40,41].

[1] C. Cercignani, *The Boltzmann Equation and Its Applications* (Springer-Verlag, New York, 1988).

[2] J. C. Maxwell, Philos. Trans. R. Soc. London **170**, 231 (1879).

[3] D. A. Lockerby, J. M. Reese, D. R. Emerson, and R. W. Baebee, Phys. Rev. E **70**, 017303 (2004).

[4] E. B. Arkilic, M. A. Schmidt, and K. S. Breuer, J. Microelectromech. Syst. **6**, 167 (1997).

[5] T. Ewart, P. Perrier, I. Geraur, and J. G. Méolans, J. Fluid Mech. **584**, 337 (2007).

[6] H. C. Weng and C. K. Chen, Phys. Fluids **20**, 106101 (2008).

 [7] R. W. Barber and D. R. Emerson, Heat Transfer Eng. **27**, 3 (2006).

 [8] C. Cercignani and A. Daneri, J. Appl. Phys. **34**, 3509 (1963).

 [9] R. G. Deissler, Int. J. Heat Mass Trans. **7**, 681 (1964).

[10] N. G. Hadjiconstantinou, Phys. Fluids **15**, 2352 (2003).

[11] S. K. Loyalka, N. Petrellis, and T. S. Steovick, Phys. Fluids **18**, 1094 (1975).

[12] C. Cegcignani and L. Fotusso, Phys. Fluids **6**, 993 (1963).

[13] C. Cercignani, M. Lampis, and S. Loeenzani, Phys. Fluids **16**, 3426 (2004).

[14] S. K. Loyalka, Phys. Fluids **18**, 1666 (1975).

[15] T. Ohwada, Y. Sone, and K. Aoki, Phys. Fluids A **1**, 1588 (1989).

[16] T. Ohwada, Y. Sone, and K. Aoki, Phys. Fluids A **1**, 2042 (1989).

[17] E. S. Oran, C. K. Oh, and B. Z. Cybyk, Annu. Rev. Fluid Mech. **30**, 403 (1998).

[18] Y. Sone, T. Ohwada, and K. Aoki, Phys. Fluids A **1**, 363 (1989).

[19] T. Kanki and S. Iuchi, Phys. Fluids **16**, 594 (1973).

[20] M. Al-Ghoul and B. C. Eu, Phys. Rev. E **70**, 016301 (2004).

[21] D. Burnett, Proc. London Math. Soc. **s2-39**, 385 (1935).

[22] S. Jin and M. Slemeod, J. Stat. Phys. **103**, 1009 (2001).

[23] M. S. Shavaliyev, J. Appl. Math. Mech. **57**, 573 (1993).

[24] M. Torrilhon and H. Struchtrup, J. Fluid Mech. **513**, 171 (2004).

[25] L. C. Woods, *An Introduction to the Kinetic Theory of Gases and Magnetoplasmas* (Oxford University Press, Oxford, 1993).

[26] X. Zhong, R. W. MacCormack, and D. R. Chapman, AIAA J. **31**, 1036 (1993).

[27] H. Brenner, Physica A **349**, 60 (2005).

[28] Z. L. Guo, B. C. Shi, and C. G. Zheng, Europhys. Lett. **80**, 24001 (2007).

[29] J. M. Li, B. X. Wang, and X. F. Peng, Int. J. Heat Mass Transfer **43**, 839 (2000).

[30] D. A. Lockerby and J. M. Reese, J. Fluid. Mech. **604**, 235 (2008).

[31] D. A. Lockerby, J. M. Reese, and M. A. Gallis, AIAA J. **43**, 1391 (2005).

[32] H. C. Ottinger, Phys. Rev. Lett. **97**, 090601 (2006).

[33] J. M. Reese, Y. Zheng, and D. A. Lockerby, J. Comput. Theor. Nanosci. **4**, 807 (2007).

[34] K. Xu, Phys. Fluids **14**, L17 (2002).

[35] C. R. Lilley and J. E. Sader, Phys. Rev. E **76**, 026315 (2007).

[36] M. Fichman and G. Hetsroni, Phys. Fluids **17**, 123102 (2005).

[37] V. K. Michalis, A. N. Kalarakis, E. D. Skouras, and V. N. Burganos, Microfluid Nanofluid **9**, 847 (2010).

[38] E. J. Arlemark, S. K. Dadzi, and J. M. Reese, J. Heat Transfer. **132**, 041006 (2010).

[39] N. Dongari, Y. Zhang, and J. M. Reese, J. Phys. D: Appl. Phys. **44**, 125502 (2011).

[40] N. Dongari, Y. Zhang, and J. M. Reese, J. Fluids Eng.-Trans. ASME **133**, 071101 (2011).

[41] N. Dongari, R. W. Barber, D. R. Emerson, S. K. Stefanov, Y. Zhang, and J. M. Reese, Microfluid Nanofluid **14**, 31 (2013).

[42] N. G. Hadjiconstantinou, Phys. Fluids **18**, 111301 (2006).

[43] C. Cercignani, M. Lampis, and S. Loeenzani, Trans. Theory Stat. Phys. **33**, 545 (2004).

[44] Z. L. Guo, B. C. Shi, and C. G. Zheng, Comput. Math. Appl. **61**, 3519 (2011).

[45] K. W. Tibbs, F. Baras, and A. L. Garcia, Phys. Rev. E **56**, 2282 (1997).

[46] J. Mathews, Phys. Fluids **21**, 876 (1978).

[47] L. F. Shampine, J. Kierzenka, and M. W. Reichelt, http://www.mathworks.com/bvp_tutorial.

[48] C. L. Bailey, R. W. Barber, D. R. Emerson, D. A. Lockerby, and J. M. Reese, AIP Conf. Proc **762**, 743 (2005).

[49] R. Goldberg, Ph.D. thesis, New York University (1954).

[50] S. A. Beresnev, V. G. Chernyak, and G. A. Fomyagin, J. Fluid Mech. **219**, 405 (1990).

[51] R. A. Millikan, Phys. Rev. **22**, 1 (1923).

[52] M. D. Allen and O. G. Raabe, Aerosol. Sci. Tech **4**, 269 (1985).

[53] K. C. Lea and S. K. Loyalka, Phys. Fluids **25**, 1550 (1982).

[54] R. W. Barber and D. R. Emerson, Tech. Rep. DL-TR-00-001, CLRC Daresbury Laboratory, 2000.